# Functional Expression of the L-Type Calcium Channel in Mice Skeletal Muscle during Prenatal Myogenesis

Caroline Strube,* Yves Tourneur,* and Carlos Ojeda†

*Laboratoire de Physiologie des Eléments Excitables, UMR Centre National de la Recherche Scientifique 5578, UCB-Lyon 1, 69622 Villeurbanne Cedex, France; and †Institut National de la Santé et de la Recherche Médicale U121, 18 avenue du doyen Lepine, 69500 Bron, France

ABSTRACT The densities of skeletal muscle intramembrane charge movement and macroscopic L-type $Ca^{2+}$ current have been shown to increase during prenatal development. In the present work, the electrophysiological characteristics of L-type $Ca^{2+}$ channels were analyzed over the embryonic period E14 to E19 using the whole-cell and cell-attached procedures. At the macroscopic level, the whole-cell L-type $Ca^{2+}$ conductance increased 100% between E14 and E19. This enhancement was accompanied by a small negative shift of the voltage dependence and a marked acceleration of the inactivation kinetics. At the single-channel level, the unitary conductance decreased significantly from 13.2 ± 0.1 pS ($n = 8$) at E14 to 10.7 ± 0.3 pS ($n = 7$) at E18 and the open probability was multiplied by 2. No significant change of the density of functional channels was observed during the same period. In contrast to the density of intramembrane charge movement, which, under the same conditions, has been shown to increase between 16 and 19 days, L-type $Ca^{2+}$ channels properties change mostly between 14 and 16 days. Taken together, these results suggest that the two functions of the dihydropyridine receptor are carried by two different proteins which could be differentially regulated by subunit composition and/or degree of phosphorylation.

## INTRODUCTION

Voltage-dependent $Ca^{2+}$ channels play an essential role in the function of skeletal muscle. The dihydropyridine (DHP) receptor of adult skeletal muscle has been postulated to serve a dual function (Rios and Brum, 1987; Tanabe et al., 1988): 1) to produce a slow, voltage-dependent $Ca^{2+}$ current identified as the L-type $Ca^{2+}$ current, and 2) to act as a voltage sensor and trigger the contractile machinery for excitation-contraction (EC) coupling. The DHP receptor is located in the cell membrane (more specifically in the transverse tubules) and is linked to the ryanodine receptor located in the sarcoplasmic reticulum membrane to form a triad (Block et al., 1988). The complex provides a structural link between surface membrane depolarization and intracellular $Ca^{2+}$ release from the sarcoplasmic reticulum. The DHP receptor is itself a complex made of four subunits: $\alpha_{1S}$, $\beta_1$, $\alpha_2/\delta$, and $\gamma$. The $\alpha_1$ subunit contains the basic functional elements of the L-type $Ca^{2+}$ channel, which include the selectivity filter, the voltage sensor and the binding sites for DHPs. The roles of the different subunits and of their mutual interactions are not completely known yet, but it has been shown that $\beta_1$, $\alpha_2/\delta$, and $\gamma$ regulate the expression of $\alpha_1$ (for review see Hofmann et al., 1994; Perez-Reyes and Schneider, 1994).

During prenatal development, skeletal muscle undergoes a number of changes in myotube morphology and in DHP receptor expression. Franzini-Armstrong (1991) showed that the initial appearance of transverse tubules, which is concomitant with the formation of the first dyads and triads, occurs fairly abruptly during prenatal development. Specific DHP binding sites ($B_{max}$) increase during fiber maturation concurrently to the development of transverse tubules (Kazazoglou et al., 1983; Schmid et al., 1984). More recently, Chaudhari and Beam (1993) showed that mRNA encoding the skeletal muscle-specific $\alpha_1$ subunit of the DHP receptor ($\alpha_{1S}$) accumulates gradually in developing skeletal muscle, whereas mRNA for the cardiac $\alpha_1$ subunit ($\alpha_{1C}$), which is present at early stages of prenatal development, diminishes rapidly in concentration as myofibers mature. During the same time, EC coupling, which depends in part on $Ca^{2+}$ influx (cardiac type) in myotubes from 14-day-old fetuses, becomes totally independent of $Ca^{2+}$ influx (skeletal type) at the end of gestation (Strube et al., 1994). The maturation of EC coupling is accompanied by a significant increase (threefold between E14 and birth) of the quantity of charge movement evoked in response to a depolarization (Strube et al., 1992) and an increase in the density of L-type $Ca^{2+}$ current (Shimahara and Bournaud, 1991).

In the present paper, we focused our study on macroscopic and unitary behavior of L-type $Ca^{2+}$ channels from mice skeletal muscle during prenatal myogenesis. We observed modifications of the properties of the L-type conductance that suggest that changes in the DHP receptor subunit composition may occur during this period of development.

## MATERIALS AND METHODS

### Single cell preparation

All experiments were performed on freshly isolated intercostal myotubes from 14- to 19-day-old mouse fetuses. Mice (Swiss OF1 from IFFA

*Received for publication 9 August 1999 and in final form 18 December 1999.*

Supported by the Centre National de la Recherche Scientifique (CNRS), the Université Claude Bernard, and the Association Française contre les Myopathies (AFM).

Address reprint requests to Caroline Strube, Laboratoire de Physiologie des Eléments Excitables, 43 bd du 11 novembre 1918, Bat 401B, 69622 Villeurbanne Cedex, France. Tel.: 33-4-72-432939; Fax: 33-4-78-946820; E-mail: strube@physio.univ-lyon1.fr.



0006-3495/00/03/1282/11 $2.00

CREDO, l'Arbresle, France) were coupled overnight. The ages of fetuses were determined by defining day 0 (E0) as that of the appearance of the plug in the morning. Pregnant mice were sacrificed by cervical dislocation and the fetuses by decapitation, in accordance with local ethical guidelines. The two half ribcages of each fetus were dissected in normal "Tyrode" solution containing (in mM) 140 NaCl, 5 KCl, 2.5 $CaCl_2$, 1 $MgCl_2$, and 10 HEPES-NaOH, pH 7.4. The tissues were incubated at 37°C for 5 to 12 min in phosphate buffered saline (Sigma, St Louis, MO), containing 3 mg/ml collagenase (type I, Sigma) and 1 mg/ml trypsin (type III, Sigma). Myotubes were then mechanically dispersed and collected in plastic petri dishes (35 mm diameter) containing Tyrode solution. Cells were maintained for at least 2 h at room temperature in Tyrode solution before the experiments were performed, also at room temperature.

## Macroscopic $Ca^{2+}$ current recordings

The standard patch-clamp technique was used in the whole-cell recording configuration. The external solution was (in mM) 130 TEA methanesulfonate, 10 $CaCl_2$, 1 $MgCl_2$, $10^{-3}$ TTX, and 10 HEPES-TEA(OH), pH 7.4. The pipette solution consisted of (in mM) 140 Cs aspartate, 5 $MgCl_2$, 10 EGTA, and 10 MOPS-CsOH, pH 7.2. Recordings were made with a RK 400 patch clamp amplifier (Bio-Logic, Claix, France). The effective series resistance was analogically compensated close to the point of amplifier oscillation. Cell capacitance was determined by integration of a capacity transient elicited by a 10-mV depolarizing pulse from holding potential–80 mV and was used to compute the $Ca^{2+}$ current densities obtained from each cell as previously described (Strube et al., 1996). The voltage drop due to series resistance (Rs × Imax) was checked for each cell and never exceeded 5 mV in the worst cases. The average value was 2.54 ± 0.13 mV ($n$ = 102). The average time lag needed to charge the membrane capacitance (Rs × Cm) was 0.83 ± 0.04 ms ($n$ = 102) and never exceeded 1.92 ms. To overcome this, the first 5–15 ms were omitted from the kinetic analysis. Data acquisition and command voltage pulse generation were performed with a Digidata 1200 interface controlled by pCLAMP software (Axon Instruments, Foster City, Ca, U.S.A.). Data were filtered at 0.3 to 1.0 kHz and digitized at 2 to 4 kHz. A 750-ms prepulse to −30 mV was used to inactivate T-type $Ca^{2+}$ current and to isolate L-type $Ca^{2+}$ current.

The voltage dependence of the $Ca^{2+}$ current density curves was fitted with a smooth curve following Eq. 1:

$$I_L(V) = G_{max}(V - V_{rev})/\{1 + \exp[(V_{G,1/2} - V)/k_G]\} \quad (1)$$

where $I_L(V)$ is the peak density of current in response to the test depolarizing potential V, $V_{rev}$ is the apparent reversal potential (determined as one of the fitted parameters), $G_{max}$ is the maximum conductance for the peak current, $V_{G,1/2}$ is the potential that elicits the half-maximum increase in conductance, and $k_G$ is a steepness parameter.

The time courses of the macroscopic L-type $Ca^{2+}$ current densities were fitted by the sum of two exponential components (Eq. 2):

$$I(t) = A_1 \times \exp(-t/\tau_1) + A_2 \times \exp(-t/\tau_2) + C \quad (2)$$

where $I(t)$ is the current density at time $t$ after the depolarization, $\tau_1$ and $\tau_2$ are the time constants for the two components of the current time course, C is the steady state current, and $A_1$ and $A_2$ are the amplitudes for each component. The quality of the fit of all the analyzed traces was evaluated with the square root of the residual variance inferior to 1.5% of the total current amplitude.

In our conditions where $\tau_1 \ll \tau_2$, Eq. 2 is an approximation of the Hodgkin and Huxley equation:

$$I = m \times h \times G_{max} \times (V - V_{rev}),$$

where $m$ and $h$ have their usual meanings (Hodgkin and Huxley, 1952).

Under these conditions,

$$C = G_{max}(V - V_{rev}) \times m_\infty \times h_\infty$$

$$A_1 = G_{max}(V - V_{rev}) \times (m_0 - m_\infty) \times h_0$$

$$A_2 = G_{max}(V - V_{rev}) \times (h_0 - h_\infty) \times m_\infty$$

Assuming that $h_0 = 1$ at −30 mV, $A_1 = G_{max}(V - V_{rev}) \times (m_0 - m_\infty)$. $A_1$ therefore reflects the fully activated L-type current density. Thus, the following Eq. 3 was used to determine the voltage dependence of the macroscopic fully activated conductance G(V):

$$G(V) = A_1(V)/(V - V_{rev}) \quad (3)$$

where $A_1(V)$ comes from Eq. 2 for a current in response to a depolarization reaching the test potential V, and $V_{rev}$ is the reversal potential determined in Eq. 1 for the concerned cell. $A_1(V)$ is taken instead of the current at the peak $I_L(V)$ because, as we will show, significant inactivation can overlap the activation phase and thus alter the apparent activation curve directly derived from the peak value.

## Single-channel measurements

Unitary $Ca^{2+}$ currents were measured using the cell-attached configuration of the standard patch-clamp technique. The bath solution was (in mM) 140 KCl, 2.5 $CaCl_2$, 1 $MgCl_2$, and 10 HEPES-KOH, pH 7.4. The pipette solution consisted of (in mM) 110 $BaCl_2$, $10^{-2}$ Bay K 8644, and 10 HEPES-TEA(OH), pH 7.4. Data were filtered at 0.3 kHz and digitized at 2 kHz. Single-channel records were digitally corrected for leak and capacitative currents by subtracting from each record the average of multiple sweeps without channel opening (blank sweeps). Ensemble averages were compiled by averaging all subtracted current records in a series. Because of the 140-mM KCl bath solution, a value of 0 mV was assumed for the resting membrane potential. All patches were held at −80 mV. Mean open current amplitudes were determined from multi Gaussian fit of current amplitude histograms.

## Variance analysis

The ensemble variance of whole-cell $Ca^{2+}$ currents was estimated from the ensemble average of the squared difference between consecutive current records as described previously (Strube et al., 1998). A set of 50 pulses to +20 mV was delivered to the same cell at a rate of 1 pulse every 10 s. The pulse cycle was delivered from a holding potential of −80 mV and consisted of a step to −30 mV for 750 ms followed by the test pulse to +20 mV followed by a step to −30 mV followed by a step to the holding potential. Test pulse duration and sampling frequency were 100 ms and 10 kHz, respectively. All records were low pass filtered at 1 kHz. Amplifier gain was set at 5 or 10 mV/pA and the A/D resolution was 1 or 0.5 pA per bit. Pairs of consecutive records were subtracted in an overlapped manner to generate 49 difference records, from which the ensemble variance was calculated. The resting variance was subtracted from the pulse variance, $\sigma^2(t)$, and the latter divided by the mean pulse current, $I(t)$. $\sigma^2(t)/I(t)$ was then plotted against $I(t)$ and the relationship was fitted according to Eq. 4:

$$\sigma^2(t)/I(t) = i - I(t)/N_F \quad (4)$$

where $i$ is the single-channel current and $N_F$ is the number of functional channels activated by the voltage pulse. Up to 20 difference records were discarded from the analysis due to deterioration of the seal resistance or excess of current run-down during the acquisition of one or both of the original pair of current records. These records were discarded without assumptions concerning the time course of the pulse variance, as described elsewhere (Strube et al., 1998).

### Curve fitting, chemicals, and abbreviations

Curve fitting was done using Marquardt-Levenberg algorithms provided by Sigmaplot (Jandel, San Rafael, CA) and pClamp (Axon Instruments, Foster City, CA). Data values are presented as means ± SE of *n* experiments. Deionized glass-distilled water was used in all solutions. All salts were reagent grade. Bay K 8644 (Calbiochem, La Jolla, CA) was made as 5 mM stocks in absolute ethanol and stored in light-resistant containers. TTX (tetrodotoxin) was from Sigma Chemical Co. Ethyleneglycol-bis-(b -aminoethyl ether) N,N,N′,N′-tetra acetic acid (EGTA), N-2-Hydroxyethyl piperazine-N′-2-ethanesulfonic acid (HEPES), 3-[N-Morpholino]propanesulfonic acid (MOPS), and tetraethylammoniun (TEA) were all from Sigma Chemical Co.

## RESULTS

In the whole-cell recordings, as expected and previously described by Shimahara and Bournaud (1991), two distinct $Ca^{2+}$ currents were clearly identified in response to 500-ms depolarizing pulses from a holding potential of −80 mV. Fig. 1 *A* shows representative records, normalized to the cell capacitance, obtained at −20 mV (upper row) where T-type current is maximum (peak of the $I_T$ = f(*V*) curve, not shown), 0 mV (middle row) where T- and L-type currents are mixed, and +20 mV (bottom row) where L-type current is largely predominant, for 14-, 16-, and 19-day-old fetuses (from left to right). T-type current density (records at −20 mV) increased between E14 and E16 and then decreased at E19; this is summarized in Fig. 1 *B*. By contrast, the L-type current density (records at +20 mV) showed a continuous increase during the same period. The ratio of L-type (at +20 mV) to T-type (at −20 mV) remained fairly constant between E14 and E16 (Fig. 1 *C*) indicating a parallel increase of T- and L-type density; the ratio increased from E16 to E19 (about threefold), mainly due to the decrease of T-type current density. These results suggest that L-type current, which is already larger than T-type current at E14 (density ratio >2), becomes even more important compared to T-type current during gestation. In the following experiments, we focused our attention on the L-type $Ca^{2+}$ current. All the whole-cell recordings were therefore done using a depolarizing prepulse to inactivate the T-type current and a 1500-ms test pulse to elicit L-type current.

Fig. 2 shows L-type $Ca^{2+}$ current recordings from myotubes of 14- (left) and 19-day-old (right) fetuses. These recordings clearly illustrate the difference in density and kinetics of the currents at 14 and 19 days; current amplitude was increased and inactivation became faster with age. As a first approach we looked at the voltage dependence of the density of L-type current at different ages. Fig. 3 *A* shows the *I-V* curves obtained with myotubes from 14-, 16-, and 19-day-old fetuses. L-type current activated around −10 mV and reached a maximum between +20 and +30 mV. The current density was smallest at all potentials at 14 days, whereas the *I-V* curves at 16 and 19 days were similar. The peak of the *I-V* curve increased during the studied period (Fig. 3 *B*). The largest increase, almost 100%, occurred between 15 and 16 days. Before 15 days and after 16 days, the maximum density of current was stable. Fitting the *I-V* curves with Eq. 1 described in methods allowed us to determine the variations with age of $G_{max}$, $V_{G,1/2}$, $k_G$, and $V_{rev}$ as shown in Fig. 3, *C, D, E,* and *F,* respectively. As expected, maximum L-type conductance varied similarly to the maximum density of L-type current. The reversal potential was constant during the studied period, suggesting

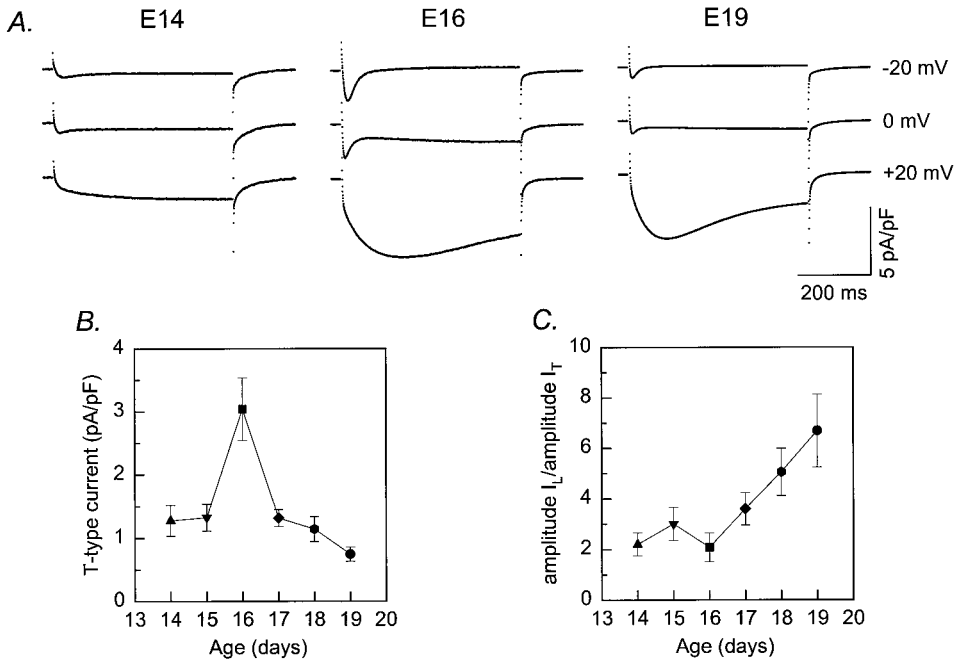


FIGURE 1 Whole-cell recordings of T- and L-type $Ca^{2+}$ currents. (*A*) $Ca^{2+}$ current recordings in response to 500-ms depolarizations from holding potential −80 mV to the indicated potentials at three different ages. Currents were normalized with respect to the cell capacitance which was 85, 186, and 720 pF at 14, 16, and 19 days, respectively. (*B*) Density of T-type current measured at the peak in response to a test pulse to −20 mV versus age of fetuses. (*C*) The amplitude of the peak of the L-type current in response to a test pulse to +20 mV was divided by the amplitude of the T-type current, and plotted versus age of fetuses. In *B* and *C*, the values are means ± SE of 8 to 11 cells at each age.

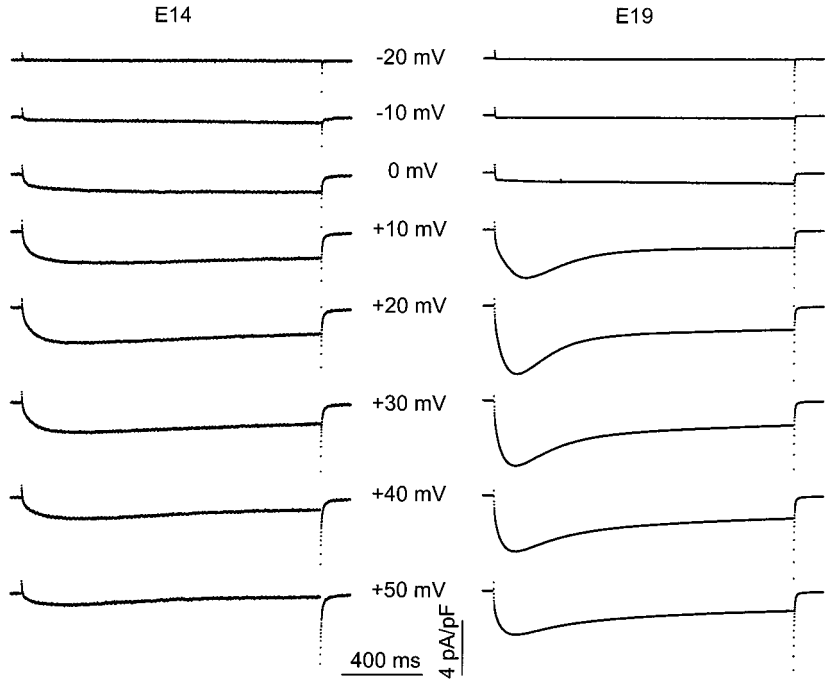


FIGURE 2 Whole-cell recordings of L-type $Ca^{2+}$ currents. L-type $Ca^{2+}$ current recorded in myotubes from 14- and 19-day-old fetuses in response to a 1500-ms step to the indicated test potential preceded by a 750-ms prepulse to −30 mV, from a holding potential of −80 mV. Currents were normalized with respect to the cell capacitance, which was 70 and 720 pF at 14 and 19 days, respectively.

that the selectivity of the channel for $Ca^{2+}$ ions did not change. Both $V_{G,1/2}$ and $k_G$ changed between 14 and 19 days. The variation of $V_{G,1/2}$ values indicates that the voltage dependence of the L-type current was shifted by about 5 mV toward more negative potentials during the last 6 days of the gestation.

To further investigate the properties of the L-type $Ca^{2+}$ current, we studied the activation and inactivation kinetics. The easiest parameter to measure is the time from the start of the pulse to the peak of the current (time to peak). Results in Fig. 4 *B* and *C* show that at all ages, time to peak was voltage-dependent for low potentials (less than +20 mV) and then stabilized for potentials more positive than +20 mV (Fig. 4 *B*). As the age increased from 14 to 19 days old there was a decrease of time to peak. This is emphasized in Fig. 4 *E*, where time to peak for $V_{test} = +30$ mV is plotted against age. The time to peak decreased dramatically between E14 and E16 (~350 to ~200 ms), followed by a much slower decrease or by stabilization. These results suggest that changes in the activation and/or inactivation kinetics of the L-type current occur during gestation. Fig. 4 *A* shows that data from macroscopic L-type current recordings (dots) can be fitted with the sum of two exponential components (continuous lines), as described in Materials and Methods (Eq. 2). In most of the cases (more than 95% of the currents obtained in response to a test pulse to a potential larger than 10 mV) Eq. 2 was sufficient to describe the current time course. The few cases where the equation did not allow a good fit of the current were obvious (square root of the residual variance around 10% of the current amplitude) and not taken into account in the averages shown in the following. Fig. 4, *C* and *D*, confirms, as seen in Fig. 4 *B*, that at all ages, kinetics were voltage-dependent for low potentials (until +20 to +30 mV) and then stabilized. Surprisingly, activation kinetics did not change with age (Fig. 4 *F*). However, the evolution of time to peak with age, seen in Fig. 4 *E*, can be explained by the variations in the inactivation kinetics. In fact, we observed an acceleration of the inactivation between 14 and 16 days, after which the values remained relatively constant until the end of gestation (Fig. 4 *G*). According to the chosen phenomenological model used to analyze our data (Hodgkin and Huxley, 1952), the reduction of time to peak described above therefore reflected the acceleration of the inactivation phase rather than the activation one. However, we cannot discard the possibility of a coupling between activation and inactivation, as proposed for sodium channels by O'Leary et al. (1995).

In order to determine whether changes in the L-type macroscopic current during myogenesis were the results of variations at the microscopic level, we studied the unitary $Ba^{2+}$ current in myotubes from 14-, 16-, and 18-day-old fetuses. Fig. 5 shows typical unitary currents recorded in cells from 14- (left) and 18-day-old (right) fetuses in presence of Bay K 8644 (10 $\mu$M) in response to 500-ms depolarizations from a holding potential of −80 mV to test potentials of 0 mV (Fig. 5 *A*), −10 mV (Fig. 5 *B*), +20 mV (Fig. 5 *C*), and +10 mV (Fig. 5 *D*). Openings of these channels were characterized by both brief and long durations. Sometimes, when the channel remained open at the end of the depolarization, single-channel tail currents were observed upon repolarization (Fig. 5, *arrows*). Ensemble

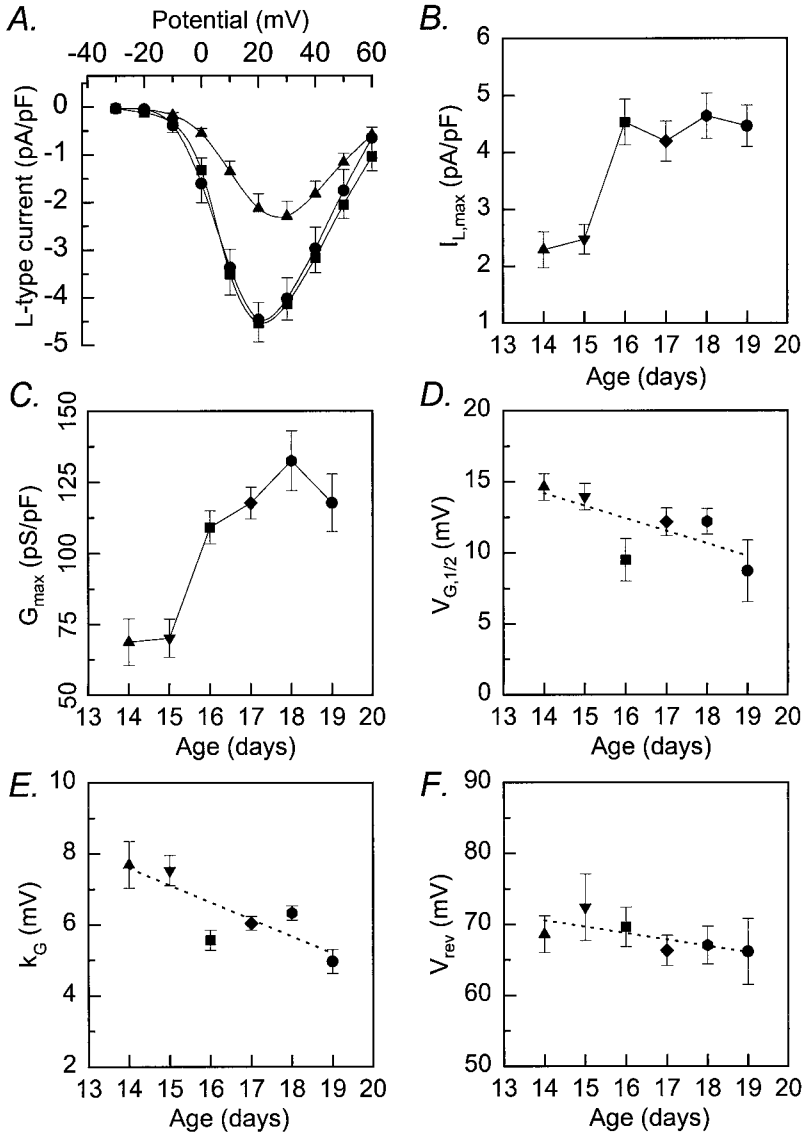


FIGURE 3 Variations of the *I-V* curve parameters in function of age. (*A*) Voltage dependence of the average L-type $Ca^{2+}$ current density measured at the peak in myotubes from 14- (*triangles, n* = 15), 16- (*squares, n* = 12), and 19-day-old (*circles, n* = 11) fetuses. (*B-F*) Average maximum L-type density *(B)*, maximum macroscopic conductance (*C*), potential that elicits the half-maximum increase in conductance (*D*), steepness factor (*E*), and reversal potential of L-type $Ca^{2+}$ current (*F*) plotted versus age of fetuses. The number of cells (*n*) used to determine the mean values at each age varied between 11 and 16.

averages displayed slow activation and inactivation, characteristic of L-type current. However, the time to peak always seemed shorter than for the whole-cell currents seen before. The main explanation is the presence of DHP agonist during single-channel measurements. In fact, in whole-cell experiments recordings (results not shown) done in presence of 10 mM $BaCl_2$ and 10 $\mu$M Bay K 8644 instead of 10 mM $CaCl_2$ display a time to peak 40 to 50% shorter. The inactivation is also obviously much faster. Moreover, Strube et al. (1998) and Dirksen and Beam (1996) showed that Bay K 8644 accelerates the activation kinetics of L-type current at a macroscopic and unitary level respectively.

Data like those shown in Fig. 5 allowed us to calculate the open probability ($p_o$) using the equation

$$p_0 = \mathrm{I}/(\mathrm{N} \times i)$$

where I is the peak ensemble current, N is the observed maximum number of simultaneously open channels, and $i$ is the single-channel current amplitude during the pulse. The calculation was done at E14 and E18 for a depolarization reaching +10 mV. We found two significantly different open probabilities ($p < 0.0025$) of 0.06 $\pm$ 0.01 ($n$ = 7) at E14 and 0.12 $\pm$ 0.02 ($n$ = 6) at E18. The latter value is consistent with that previously reported for skeletal L-type $Ca^{2+}$ channels from cultured myotubes measured in the presence of 110 mM $Ba^{2+}$ and Bay K 8644 (Dirksen and Beam, 1995).

Fig. 6 *A* shows all point amplitude histograms from the same patches as in Fig. 5, *B* and *D*. Amplitude histograms were fitted by the sum of either three (Fig. 6 *A*) or four (Fig. 6 *B*) Gaussian distributions. In both histograms, the large peak near 0 pA represents the current level when all chan-

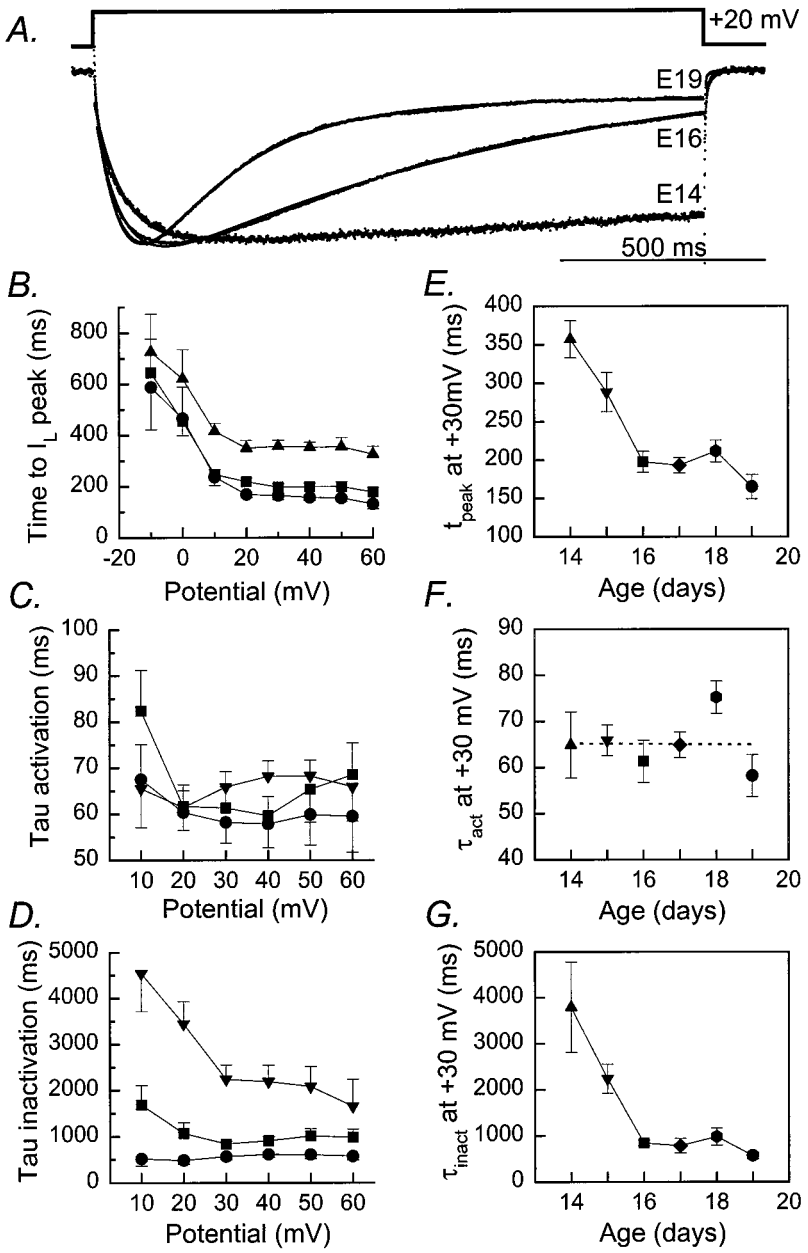


FIGURE 4 Kinetics of activation and inactivation of the L-type $Ca^{2+}$ current. (*A*) Traces of $Ca^{2+}$ current recorded (normalized with respect to the peak) in myotubes from 14-, 16-, and 19-day-old fetuses in response to a 1500-ms depolarizing pulse to +20 mV. The solid curve correspond to a fit using Eq. 2 described in Materials and Methods with C = −0.018, $A_1$ = 0.8, $A_2$ = −0.8, $\tau_1$ = 69.8 ms, $\tau_2$ = 6.36 s at E14, C = 0.05, $A_1$ = 1.1, $A_2$ = −1.4, $\tau_1$ = 67.5 ms, $\tau_2$ = 0.97 s at E16, and C = −0.17, $A_1$ = 1.9, $A_2$ = −1.9, $\tau_1$ = 64.1 ms, $\tau_2$ = 0.23 s at E19. (*B*) Voltage dependence of the time to peak in myotubes from 14- (*triangles, n* = 15), 16- (*squares, n* = 12), and 19-day-old (*circles, n* = 11) fetuses. (*C, D*) Voltage dependence of the activation *(C)* and inactivation (*D*) time constant of the L-type current recorded in myotubes from 15- (*triangles, n* = 11), 16- (*squares, n* = 12), and 19-day-old (*circles, n* = 9) fetuses. (*E-G*) Average time to peak *(E)*, activation rate (*F*), and inactivation rate (*G*) at +30 mV versus age of fetuses. The number of cells (*n*) used to determine the mean values at each age varied between 7 and 16.

nels are closed. The other peaks occurred in multiples of ~0.73 pA and ~0.52 pA for pulses reaching −10 mV and +10 mV, respectively, and proportionally favored the lower amplitude peaks. These data agree with the presence of three identically conducting channels in the patch rather than the presence of substate conductances. The analysis of all point amplitude histograms for different depolarizations (from a holding potential of −80 mV) allowed us to determine the unitary channel conductance at different ages. Fig. 6 *B* shows the voltage dependence of single-channel amplitude at 14, 16, and 18 fetal days. The slopes of the fitted lines gave the unitary conductance at each age. The average unitary conductance (Fig. 6 *C*) for channels found in myotubes from 16- and 18-day-old fetuses were the same (10.7 ± 0.7 pS, $n$ = 6, and 10.7 ± 0.3 pS, $n$ = 7, respectively), whereas the unitary conductance was significantly larger (unpaired $t$-test, $p < 0.002$) at 14 days (13.2 ± 0.1 pS, $n$ = 8). These values are close to those previously described by Dirksen and Beam (1995) in cultured skeletal muscle myotubes. It should be noted that the unitary conductance decreased between E14 and E16, whereas during this period the macroscopic conductance increased. The unitary conductances were always smaller than those described for the expression of $\alpha_{1C}$ in skeletal muscle cells from dysgenic mice (~25 pS, Dirksen and Beam, 1995). This suggests that, although at early ages EC coupling is

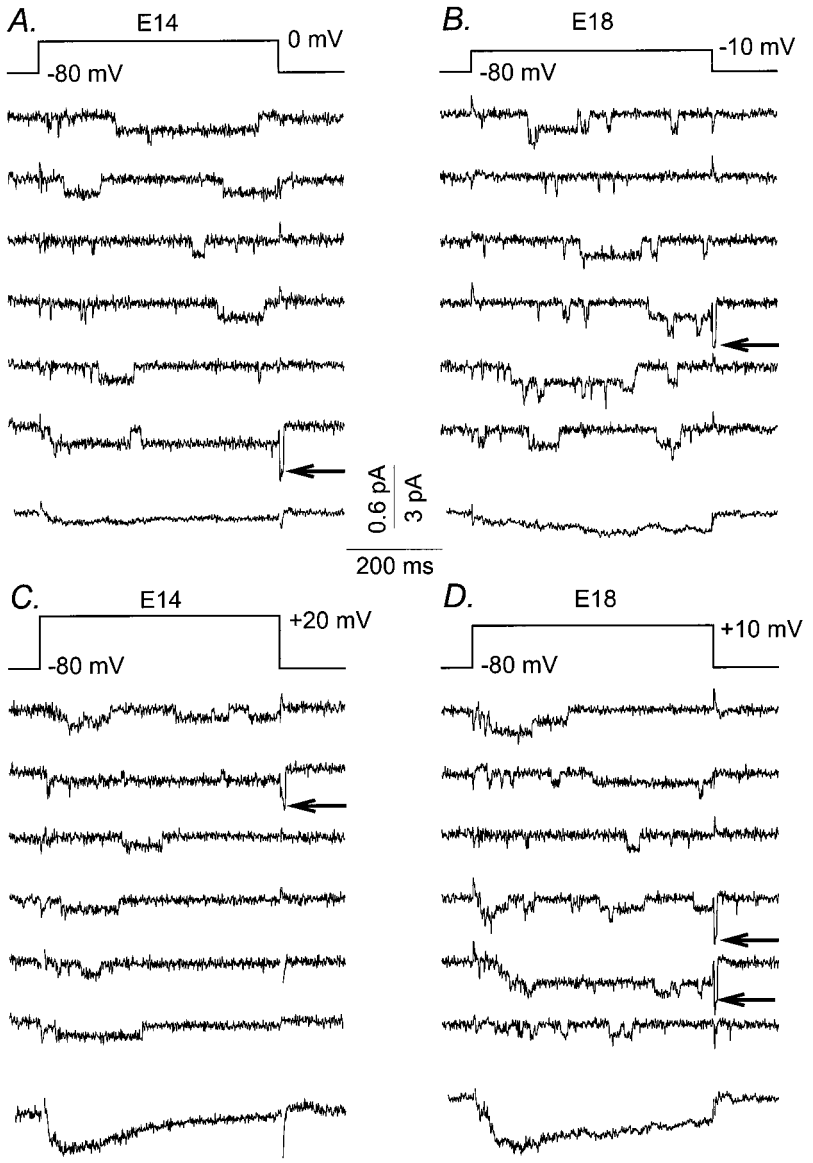


FIGURE 5 Single-channel recordings of the L-type current. *Middle of each panel:* Selected sweeps of unitary $Ba^{2+}$ current recorded from myotubes at E14 (*A* and *C*) and E18 (*B* and *D*). Vertical calibration is 3 pA. *Arrows* indicate single-channel tail currents. *Top of each panel:* The voltage protocol consisted of a 500-ms depolarizing pulse from a holding potential of −80 mV to the indicated potential. *Bottom of each panel:* Ensemble averages of around 100 individual sweeps. Vertical calibration is 0.6 pA.

close to the cardiac type, the unitary L-type conductance characterized here was clearly different from that of the cardiac isoform of $\alpha_1$, $\alpha_{1C}$.

The last parameter we estimated using mean-variance analysis is the density of functional $Ca^{2+}$ channels. Fig. 7 *A* shows the time course of the mean whole-cell $Ca^{2+}$ current (smooth trace) and its intrinsic variance (noisy trace) in response to a test pulse to +20 mV at E14 and E18. The mean currents and the ensemble variances shown in Fig. 7 were averaged for 7 cells at E14 and for 7 cells at E18. At both ages, the variance increased with the mean current throughout the pulse. Fig. 7 *B* shows variance/mean current ratio plotted as a function of the mean current for the same data. The parameters of the linear fit of the data according to Eq. 4 are given in the figure legend. The values of $i$ and $N_F$ are consistent with previous determination in normal cultured myotubes (Strube et al., 1998). The slightly smaller values found for the density of channels, $N_F$, could be explained by the difference of preparation (culture versus fresh cells). To provide for a statistical test of the data, we estimated $i$ and $N_F$ for each cell separately. The mean values for $i$ are 0.047 ± 0.006 pA ($n$ = 7), 0.035 ± 0.006 pA ($n$ = 5) and 0.034 ± 0.004 pA ($n$ = 7) at E14, E16 and E18 respectively. The values of $N_F$ are 185 ± 44 channels/pF ($n$ = 7), 288 ± 101 channels/pF ($n$ = 5) and 221 ± 28 channels/pF ($n$ = 7) at E14, E16, and E18, respectively. Neither $i$ nor $N_F$ were significantly different two-by-two according to an unpaired $t$-test. According to the results obtained with single-channel recordings (small change in the L-type $Ca^{2+}$ channel unitary conductance during gestation), together with the fact that the whole-cell recordings were done in presence of only 10 mM $Ca^{2+}$, the absence of

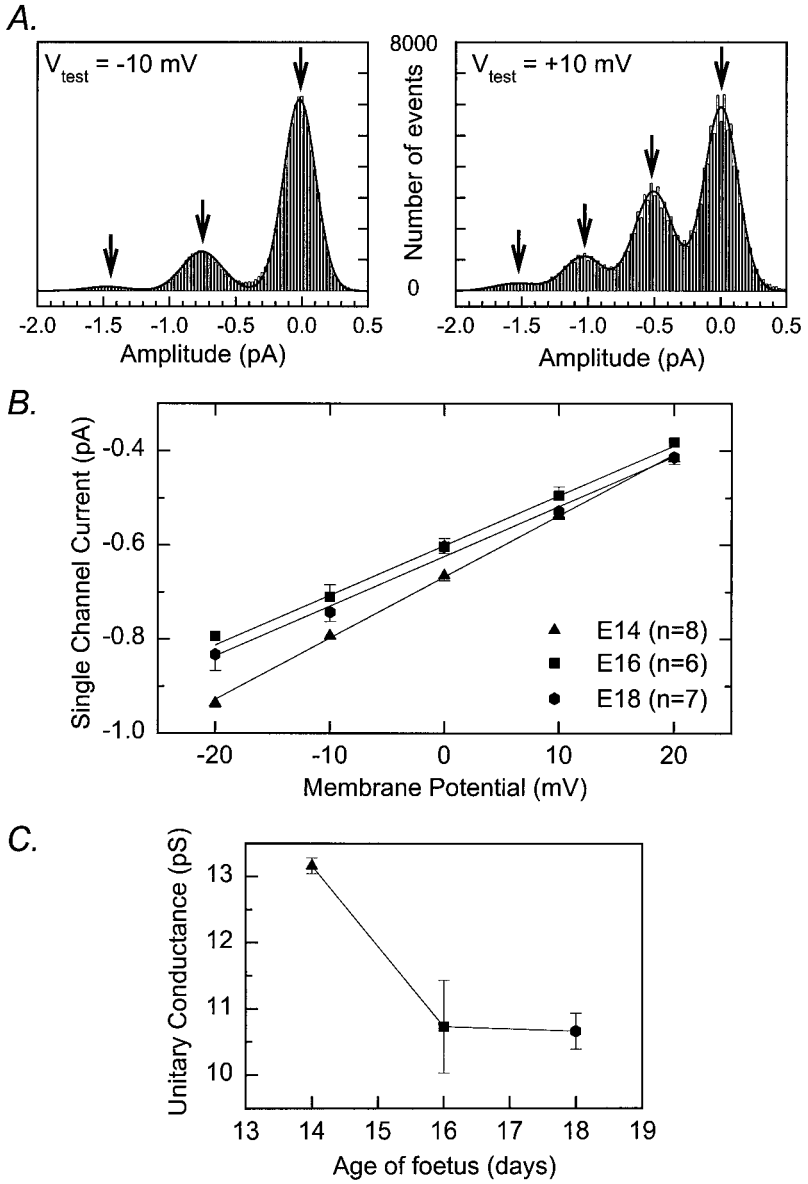


FIGURE 6 Single-channel conductance of the L-type current. (*A*) All point amplitude histograms at −10 mV (*left*) and +10 mV (*right*) taken from the experiments shown in Fig. 5, *B* and *D*. Each histogram was constructed from around 150 traces. The smooth curve represents the best fit of the sum of three (*left*) or four (*right*) Gaussian distributions (*arrows*). The fitted parameters for central value ($\mu$) and standard deviation ($\sigma$) were (in pA): (*left*) $\mu_1 = -0.017$, $\sigma_1 = 0.122$, $\mu_2 = -0.754$, $\sigma_2 = 0.151$, $\mu_3 = -1.470$, $\sigma_3 = 0.152$; (*right*) $\mu_1 = 0.002$, $\sigma_1 = 0.128$, $\mu_2 = -0.507$, $\sigma_2 = 0.146$, $\mu_3 = -1.032$, $\sigma_3 = 0.146$, $\mu_4 = -1.533$, $\sigma_4 = 0.176$. The Gaussian distributions were represented by peaks, which occurred in multiples of ~0.73 (*left*) and ~0.52 pA (*right*). A single-channel conductance of 11.2 pS was calculated using these and three similar histograms constructed from a total of five different voltages. (*B*) Voltage dependence of average single-channel current from a total of 8 (E14), 6 (E16), and 7 (E18) different patches from different cells. Typically, depolarizations to potentials lower than −20 mV could not elicit openings, and depolarizations to potentials larger than 20 mV elicited openings too small to be analyzed. A linear regression of the data revealed a single-channel conductance of 13.0 pS (E14), 10.4 pS (E16), and 10.5 pS (E18). (*C*) Average single-channel conductance versus age of fetuses.

any significant difference in the elementary current determined in the whole-cell variance analysis experiments is not aberrant. Concerning the density of channels, we cannot exclude small changes that may have been masked by the lack of accuracy of the variance analysis technique.

## DISCUSSION

The present results, in agreement with previous work (Beam and Knudson, 1988; Shimahara and Bournaud, 1991), show that the amplitude of T- and L-type $Ca^{2+}$ currents varies during skeletal muscle development. Additionally, we show for the first time that the biophysical characteristics of L-type channels undergo important changes during myogenesis. Between 14 and 19 prenatal days, the macroscopic L-type current density increased. In contrast, the density of T-type current underwent a transient change, because it reached a maximum (3 pA/pF) in myotubes from 16-day-old fetuses. At present, the role of the T-type $Ca^{2+}$ current in skeletal muscle remains undetermined, but this current may be differentially involved in prenatal myogenesis before and after the key age of 16 days. To further analyze the increase in L-type $Ca^{2+}$ current density, we looked at the macroscopic fully activated conductance at 14 and 19 days. The maximum conductance ($G_{max}$, Fig. 3 *C*) and the potential at which the conductance is half-maximally activated ($V_{G,1/2}$, Fig. 3 *D*), computed from the peak current I/V curve (Eq. 1), might suggest a negative shift of the activation curve. A better estimate is obtained from the analysis of the time-dependent current (i.e., Eq. 3). The results of such a calculation, shown in Fig. 8, clearly demonstrate the increase (by about a factor of 2) in the maximum macroscopic

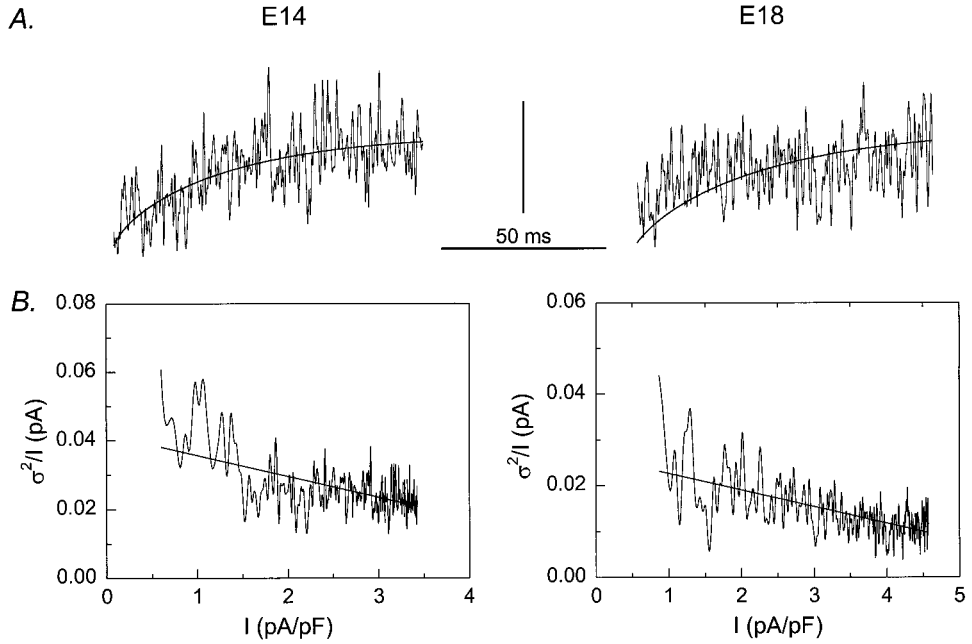


FIGURE 7 Variance-current relationship of the L-type $Ca^{2+}$ current. (*A*) Superimposed time courses of the mean whole-cell $Ca^{2+}$ current (*smooth traces*) and the ensemble variance (*noisy trace*) in response to a 100-ms step potential to +20 mV. Traces correspond to average of 7 cells from 14-day-old fetuses and 7 cells from 18-day-old fetuses. Vertical calibration bar corresponds to I = 3 pA/pF and $\sigma^2$ = 0.05 $pA^2$/pF at E14 and I = 4 pA/pF and $\sigma^2$ = 0.05 $pA^2$/pF at E18. (*B*) Ensemble variance/mean current ratio plotted as a function of the mean current for the same averages. The smooth lines are a fit of the data according to Eq. 4 with parameters $i$ = 0.04 pA and $N_F$ = 167/pF at E14 and $i$ = 0.03 pA and $N_F$ = 269/pF at E18.

conductance at E19 compared to E14 and also illustrate the changes of $V_{1/2}$.

The macroscopic conductance G is defined as G (pS/pF) = $\gamma$ (pS) × $N_F$ ($pF^{-1}$) × $p_o$, with $\gamma$ being the unitary conductance, $N_F$ being the total density of functional channels in the cell membrane, and $p_o$ the probability that those channels are open. The shift of the activation curve can be explained by changes in the voltage dependence of $p_o$. We have shown that $\gamma$ decreases by about 2.5 pS, which implies

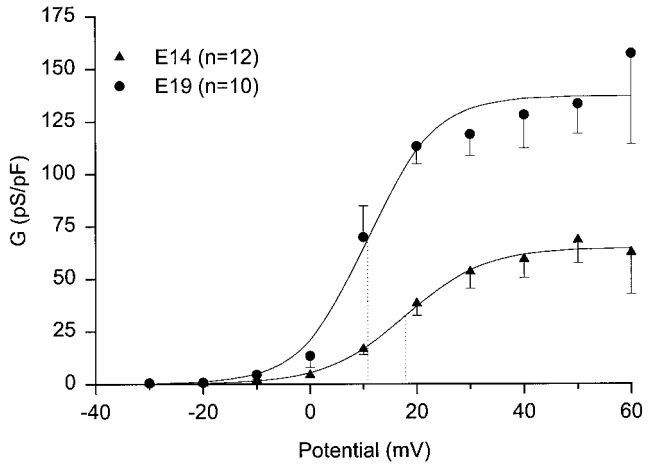


FIGURE 8 Voltage dependence of the L-type $Ca^{2+}$ macroscopic conductance. Voltage dependence of average L-type current macroscopic conductance in myotubes from 14- (*triangle, n* = 12) and 19-day-old (*circles, n* = 10) fetuses. The values for each cell are obtained from Eq. 3 as described in Materials and Methods. The parameters of the fit (*continuous lines*) using Boltzmann equation are $G_{max}$ = 65 and 137 pS/pF, $V_{1/2}$ = 17.9 and 10.8 mV, and k = 7.4 and 6.3 mV at E14 and E19, respectively. The *dotted lines* indicate the shift of $V_{1/2}$.

that the increase in G at all studied potentials is due to an increase of N × $p_o$ (density of functional open channels). The two independent observations showing that the open probability is multiplied by 2 and that the density of functional channels does not change significantly during the studied period are consistent with the 100% increase of $G_{max}$ seen during the same period. All these results suggest that the increase of $G_{max}$ is mostly due to an increase in the open probability accompanied by a small decrease in the unitary conductance. As said in the Results section, we cannot exclude small changes in the density of functional channels. However, our results discard the hypothesis that the observed change in maximum macroscopic conductance is due to a drastic change in the density of channels. At first sight, the latter statement seems to contradict the increase in the quantity of mRNA encoding for skeletal muscle $\alpha_1$ subunit seen by Chaudhari and Beam (1993) and the increase of $B_{max}$ observed in DHP binding experiments (Kazazoglu et al., 1983; Schmid et al., 1984). But a closer analysis of the situation can explain this apparent discrepancy. In fact, this absence of significant change of the density of L-type $Ca^{2+}$ channels (DHP receptors permeant to $Ca^{2+}$), together with the increase of the density of nifedipine-sensitive charge movement (carried by DHP receptors) shown by Strube at al. (1992) during the same prenatal period, suggests the presence of two different types of DHP receptors which may be differentially regulated, each carrying one function. One type of receptor would be permeant to $Ca^{2+}$ ions and serve as an L-type $Ca^{2+}$ channel without being directly involved in the EC coupling. The other type of receptor would be the voltage sensor for EC coupling but would not conduct any transmembrane current. In such a

case, the mRNA increasing during the prenatal period would be coding for the EC coupling voltage sensor, and the increase of the quantity of mRNA (between 14 and 17 days of fetal development) would precede the increase of the density of protein producing charge movement (mostly between E16 and E19). The hypothesis that one type of DHP receptor carries both functions seems hard to defend. The increase in the density of charge movement, which occurs after the increase of the density of current without significant change in the density of functional channels, would suppose a higher number of functional charges per receptor. This could result from the formation of dyads and triads, which occurs at the same time (Franzini-Armstrong, 1991) and introduces additional interactions between the DHP receptor and other proteins, such as the ryanodine receptor. However, Nakai et al. (1996) showed that the presence of ryanodine receptors enhances the function of DHP receptors as $Ca^{2+}$ channels without effect on charge movement. Thus, the only way to explain all these observations taken together would be an overproduction of DHP receptors in relation to the number of available ryanodine receptors. This seems unlikely, however, if we consider the fact that charge movements carried by DHP receptors are implicated in EC coupling and then expected to interact with ryanodine receptors.

At the macroscopic level, we noted an acceleration of the time to peak of the L-type current with development. For a depolarization to +30 mV, there was a strong correlation ($r = 0.51$) between time to peak and current density (results not shown), which could be compared to the positive correlation between channel density and activation speed seen by Adams et al. (1996). However, our results demonstrate that the analysis of the time to peak of the current cannot be assimilated to the activation rate if any inactivation occurs. In our experiments, the inactivation is fast enough to account for the observed changes in time to peak with age, whereas in the paper by Adams et al. (1996), the pulses are too short to conclude whether inactivation and activation kinetics overlap. The acceleration of the inactivation kinetics with age occurs concomitantly with the increase of the amplitude of the $Ca^{2+}$ current, which implies more $Ca^{2+}$ entering the cell and could justify a larger $Ca^{2+}$-dependent inactivation. All recordings were made with 10 mM EGTA in the pipette, which may not have ensured a rapid and complete subsarcolemmal $Ca^{2+}$ buffering. However there is no correlation ($r^2 = 0.045$, results not shown) between the inactivation rate ($\tau_2$ from Eq. 2) and the $Ca^{2+}$ influx approximated by the area between the baseline and the current trace I(t) (i.e., integration of the total current, which represents the amount of charges flowing through the membrane). Moreover, the inactivation rate values plotted versus the potential (Fig. 5 *C*) do not display a U-shaped curve, indicating that even when there is less $Ca^{2+}$ entry for high potentials, the inactivation does not slow down. All these observations taken together suggest that the decrease in the inactivation time constant is due not to a larger entry of $Ca^{2+}$ in E19 versus E14 cells but rather to a change in the intrinsic properties of the $Ca^{2+}$ channel.

The changes in unitary conductance, open probability of the single channel, and inactivation kinetics of the whole-cell current suggest alterations in the intrinsic properties of L-type $Ca^{2+}$ channel. We have mentioned above that interaction with other proteins and with the ryanodine receptor in particular (Nakai et al., 1996) can modulate the $Ca^{2+}$ channel function of the DHP receptor. However, with the first triads appearing around E16, this interaction seems to take place rather late. Thus, changes in the subunit molecular composition of the DHP receptor seem a more likely explanation of the alterations of $Ca^{2+}$ current properties. More specifically, one can envisage the presence of different $\alpha_1$ subunits during myogenesis and/or modifications of the interactions between the $\alpha_{1S}$ subunit and the other subunits that constitute the DHP receptor. Concerning the nature of $\alpha_1$, Chaudhari and Beam (1993) showed that the mRNA encoding for the cardiac type of $\alpha_1$, $\alpha_{1C}$, is detectable at high concentration in muscles from 14-day-old fetuses, but diminishes rapidly during prenatal development. Bulteau et al. (1998) even showed that the mRNA encoding for $\alpha_{1C}$ expressed in rat skeletal muscle cells in primary culture can function as a calcium channel. However, the presence of $\alpha_{1C}$ in the membrane at early stages of gestation cannot explain the slower time to peak seen in younger myotubes compared to older ones, because $\alpha_{1C}$ has a faster activation and inactivation than $\alpha_{1S}$ (Tanabe et al., 1990; McDonald et al., 1994). Most of all, the single-channel conductance of $\alpha_{1C}$ expressed in dysgenic muscle is larger than that of $\alpha_{1S}$ (~25 pS vs. ~14 pS, Dirksen and Beam, 1996). During cell-attached patch recordings, we never observed a conductance level which could have arisen from the expression of $\alpha_{1C}$, suggesting that $\alpha_{1C}$ was either absent or not functional in our preparation. This negative result cannot be related to a location of $\alpha_1$ within the T-tubules, because the tubular system develops only after the 16th day of gestation and appears gradually over a period of about 3 weeks (Franzini-Armstrong, 1991), suggesting that T-tubules are not yet well developed even at E19. Taken together, the above observations favor a molecular modulation of $\alpha_{1S}$, which is more likely due to changes in the regulatory subunit composition of the DHP receptor than to a change in the nature of $\alpha_1$. This hypothesis is supported by previous work showing that $\beta$, $\alpha_2/\delta$, and $\gamma$ subunits can regulate the expression of $\alpha_1$. For example, Varadi et al. (1991) showed that the presence of the $\beta$ subunit accelerates activation and inactivation kinetics of the skeletal muscle $Ca^{2+}$ channel current expressed in L cells. The same year, Singer et al. (1991) reported pronounced effects of skeletal muscle $\alpha_2/\delta$, $\beta$, and $\gamma$ subunits on macroscopic amplitude, kinetics, and voltage dependence of the $Ca^{2+}$ current produced by the expression of $\alpha_{1C}$ in oocytes. Eberst et al. (1997) also reported an acceleration of the inactivation of the $\alpha_{1C}$ current by the $\gamma$ subunit. At the single-channel level, $\beta$ (Gerster

et al., 1999) and $\alpha_2/\delta$ (Shistik et al., 1995) subunits have been reported to be able to modulate the single-channel open probability of the $\alpha_{1C}$ pore-forming subunit. All these observations support the hypothesis of an alteration of skeletal L-type current properties due to a modulation of $\alpha_{1S}$ by other subunits. Moreover, such a regulation of protein expression depending on the subunit composition has already been shown during muscle development by Mishina et al. (1986) for the acetylcholine receptor, which changes conductance and gating properties with the replacement of the $\gamma$ subunit by the $\epsilon$ subunit. An alternative explanation of the alterations in L-type $Ca^{2+}$ channels properties during embryogenesis could be a change of the degree of channel modulation. For example, Delbono et al. (1997) showed that insulin-like growth factor-1 increases $Ca^{2+}$ current amplitude and shifts the I-V curve toward more negative potentials via a phosphorylation mechanism without effect on charge movement. One can imagine that one type of DHP receptor, carrying the EC coupling voltage sensor, is not affected by phosphorylation, whereas the degree of phosphorylation of the other one, serving as L-type $Ca^{2+}$ channel, is modulated during myogenesis.

We thank Roberto Coronado for judicious advice, Oger Rougier for helpful comments, and Isabel Ann Lefevre for critical reading of the manuscript.

## REFERENCES


Adams, B. A., T. Tanabe, and K. G. Beam. 1996. $Ca^{2+}$ current activation correlates with $\alpha_1$ density. *Biophys. J.* 71:156–162.

Beam, K. G., and C. M. Knudson. 1988. Effect of postnatal development on calcium current and slow charge movement in mammalian skeletal muscle. *J. Gen. Physiol.* 91:799–815.

Block, B., T. Imagawa, K. P. Campbell, and C. Franzini-Armstrong. 1988. Structural evidence for direct interaction between the molecular components of the transverse tubule/sarcoplasmic reticulum junction in skeletal muscle. *J. Cell Biol.* 107:2587–2600.

Bulteau, L., G. Raymond, and C. Cognard. 1998. Antisense oligonucleotides against "cardiac" and "skeletal" DHP-receptors reveal a dual role for the "skeletal" isoform in EC coupling of skeletal muscle cells in primary culture. *J. Cell Sci.* 111:2149–2158.

Chaudhari, N., and K. G. Beam. 1993. mRNA for cardiac calcium channel is expressed during development of skeletal muscle. *Dev. Biol.* 155: 507–515.

Delbono, O., M. Renganathan, and M. L. Messi. 1997. Regulation of mouse skeletal muscle L-type $Ca^{2+}$ channel by activation of the insulin-like growth factor-1 receptor. *J. Neurosci.* 15:6918–6928.

Dirksen, R. T., and K. G. Beam. 1995. Single calcium channel behavior in native skeletal muscle. *J. Gen. Physiol.* 105:227–247.

Dirksen, R. T., and K. G. Beam. 1996. Unitary behavior of skeletal, cardiac, and chimeric L-type $Ca^{2+}$ channels expressed in dysgenic myotubes. *J. Gen. Physiol.* 107:731–742.

Eberst, R., S. Dai, N. Klugbauer, and F. Hofmann. 1997. Identification and functional characterization of a calcium channel $\gamma$ subunit. *Pflügers Arch. Eur. J. Physiol.* 433:633–637.

Franzini-Armstrong, C. 1991. Simultaneous maturation of transverse tubules and sarcoplasmic reticulum during muscle differentiation in the mouse. *Dev. Biol.* 146:353–363.

Gerster U., B. Neuhuber, K. Groschner, J. Striessnig, and B. E. Flucher. 1999. Current modulation and membrane targeting of the calcium channel alpha1C subunit are independent functions of the beta subunit. *J. Physiol. (Lond.)* 517:353–368.

Hodgkin, A. L., and A. F. Huxley. 1952. A quantitative description of membrane current and its application to conduction and excitation in nerve. *J. Physiol. (Lond.)* 117:500–544.

Hofmann, F., M. Biel, and V. Flockerzi. 1994. Molecular basis for $Ca^{2+}$ channel diversity. *Ann. Rev. Neurosci.* 17:399–418.

Kazazoglou, T., A. Schmid, J.-F. Renaud, and M. Lazdunski. 1983. Ontogenic appearance of $Ca^{2+}$ channels characterized as binding sites for nitrendipine during development of nervous, skeletal and cardiac muscle systems in the rat. *FEBS Lett.* 164:75–79.

McDonald, T. F., S. Pelzer, W. Trautwein, and D. J. Pelzer. 1994. Regulation and modulation of calcium channels in cardiac, skeletal, and smooth muscle cells. *Physiol. Rev.* 74:365–507.

Mishina, M., T. Takai, K. Imoto, M. Noda, T. Takahashi, S. Numa, C. Methfessel, and B. Sakmann. 1986. Molecular distribution between fetal and adult forms of muscle acetylcholine receptor. *Nature.* 321:406–411.

Nakai, J., R. T. Dirksen, H. T. Nguyen, I. N. Pessah, K. G. Beam, and P. D. Allen. 1996. Enhanced dihydropyridine receptor channel activity in the presence of ryanodine receptor. *Nature.* 380:72–75.

O'Leary, M. E., L.-Q. Chen, R. G. Kallen, and R. Horn. 1995. Molecular link between activation and inactivation of sodium channels. *J. Gen. Physiol.* 106:641–658.

Perez-Reyes, E., and T. Schneider. 1994. Calcium channels: structure, function and classification. *Drug Dev. Res.* 33:295–318.

Rios, E., and G. Brum. 1987. Involvement of dihydropyridine receptor in excitation-contraction coupling in skeletal muscle. *Nature.* 325: 717–720.

Schmid, A., J-F. Renaud, M. Fosset, J-P. Meaux, and M. Lazdunski. 1984. The nitrendipine sensitive $Ca^{2+}$ channel in chick muscle cells and its appearance during myogenesis in vitro and in vivo. *J. Biol. Chem.* 259:11366–11372.

Shimahara, T., and R. Bournaud. 1991. Barium current in developing skeletal muscle cells of normal and mutant mice fetuses with "muscular dysgenesis". *Cell Calcium.* 12:727–733.

Shistik, E., T. Ivanina, T. Puri, M. Hosey, and N. Dascal. 1995. $Ca^{2+}$ current enhancement by alpha2/delta and beta subunits in Xenopus oocytes: contribution of changes in channel gating and alpha1 protein level. *J. Physiol. (Lond.)* 489:55–62.

Singer, D., M. Biel, I. Lotan, V. Flockerzi, F. Hofmann, and N. Dascal. 1991. The roles of the subunits in the function of the calcium channel. *Science.* 253:1553–1557.

Strube, C., M. Beurg, D. Georgescauld, R. Bournaud, and T. Shimahara. 1994. Extracellular $Ca^{2+}$-dependent and independent calcium transient in fetal myotubes. *Pflügers Arch. Eur. J. Physiol.* 427:517–523.

Strube, C., M. Beurg, P. A. Powers, R. G. Gregg, and R. Coronado. 1996. Reduced $Ca^{2+}$ current, charge movement, and absence of $Ca^{2+}$ transients in skeletal muscle deficient in dihydropyridine receptor beta 1 subunit. *Biophys. J.* 71:2531–2543.

Strube, C., M. Beurg, M. Sukhareva, C. A. Ahern, J. A. Powell, P. A. Powers, R. G. Gregg, and R. Coronado. 1998. Molecular origin of the L-type $Ca^{2+}$ current of skeletal muscle myotubes selectively deficient in dihydropyridine receptor $\beta_1$ subunit. *Biophys. J.* 75:207–217.

Strube, C., R. Bournaud, I. Inoue, and T. Shimahara. 1992. Intramembrane charge movement in developing skeletal muscle cells from fetal mice. *Pflügers Arch. Eur. J. Physiol.* 421:572–577.

Tanabe, T., K. G. Beam, J. A. Powell, and S. Numa. 1988. Restoration of excitation-contraction coupling and slow calcium current in dysgenic muscle by dihydropyridine receptor complementary DNA. *Nature.* 336: 134–139.

Tanabe, T., A. Mikami, S. Numa, and K. G. Beam. 1990. Cardiac-type excitation-contraction coupling in dysgenic skeletal muscle injected with cardiac dihydropyridine receptor cDNA. *Nature.* 344:451–453.

Varadi, G., P. Lory, D. Schultz, M. Varadi, and A. Schwartz. 1991. Acceleration of activation and inactivation by the $\beta$ subunit of the skeletal muscle calcium channel. *Nature.* 352:159–162.